Two-dimensional Josephson junction arrays with dc drives: The fixed-point regime

Shantilal Das, Sujay Datta, and Deshdeep Sahdev
Department of Physics, Indian Institute of Technology, Kanpur 208 016, India

Ravi Mehrotra
National Physical Laboratory, Dr. K. S. Krishnan Road, New Delhi 110 012, India

(Received 1 August 1996)

A fixed-point analysis of two-dimensional Josephson junction arrays subject to dc drives is carried out analytically, at a zero temperature and in a zero magnetic field. Conditions for the existence and stability of such behavior are established, by studying in detail, the isolated triangular and square plaquette. The results are subsequently generalized to Josephson junction ladders and rectangular arrays which could contain linear defects. We deduce a closed form inductive expression for the critical surface in the space of phase configurations. All the analytic results are checked against numerical simulations. [S1063-651X(97)08402-X]

PACS number(s): 05.45+b, 74.40.+k, 74.50.+r

I. INTRODUCTION

The dynamical properties of Josephson junction arrays (JJAs) have recently been the focus of experimental [1–7] and numerical studies [8–15], which have resulted in several insights. To cite an example of interest for this paper, it has come to be appreciated that in dc-driven JJAs at zero temperature and zero magnetic field, a transition from superconductive to resistive current flow invariably occurs through a flow of vortices perpendicular to the external current [8,12]. The situation is the same as in continuous superconductors except for the following differences. Firstly, the self-induced magnetic field, which plays a crucial role in the continuum, is for all practical purposes absent in a number of experimental JJAs. Secondly, the discrete nature of the JJA provides a natural pinning potential for vortices [16], because of which, the breakdown of superconductive flow occurs only when the driving current exceeds the depinning current of the array at *every* point along the vortex path [17]. This breakdown can be observed in uniformly driven arrays with defects [8,14], as also in uniformly driven perfect arrays at finite temperatures and/or in nonzero magnetic fields [9,10]. Alternatively, we could consider perfect arrays at zero temperature and zero magnetic field, but make the drive nonuniform [11–13]. Each of these situations contains a natural mechanism for the injection of vortices as also the current drive to set these into motion. It has, furthermore, been noticed that the critical value of the external drive, for which the transition occurs, depends both on how the drive is applied and how the array boundaries are configured (a missing bond, in this context, should be thought of as introducing an internal boundary).

A fixed-point analysis which could help systematize these insights and analytically determine some of the associated dynamical quantities, has, however, not been carried out for JJAs. It is evident that, much as this analysis, for the equations modeling the system, is trivial at the level of a single junction, it rapidly grows in complexity as the size of the network increases and the number of independent degrees of freedom proliferate. It is thus, *a priori*, unclear whether it is at all possible to describe the fixed points of arbitrary JJAs through expressions which are in any way tractable.

It is the aim of this paper to show that this can actually be done, at least for dc-driven JJAs at zero temperature and zero magnetic field. To demonstrate this, it is expedient to proceed in steps. We accordingly study the triangular and square plaquettes in detail, before moving onto vertical ladders with bus-bars at one end, and finally to rectangular arrays which could contain linear defects. In each of these cases, we are able to develop a closed-form inductive expression for the critical surface in the space of phase configurations. This involves the vanishing of a functional $D_n(\{\phi_r\})$ which assigns a real number to a given phase configuration $\{\phi_r\}$. The functional D_n can, as we shall see, be treated as an order parameter. We shall, furthermore, provide examples of how D_n can be used to extract analytic information.

We reiterate that our analysis pertains to zero temperature, i.e., to a situation in which thermal fluctuations have been frozen out. It is because of this that the equations of motion produce a unique fixed point, once the current drive has been specified. At finite temperatures, the situation is no longer deterministic and fluctuations occur with well-defined probabilities, around the ground states we describe. These states can be modified further by applying a static magnetic field in addition to the current drive. Finally, in the limit of large arrays our system is a driven *field* defined on a lattice.

The paper is organized as follows. In Sec. II, we put down the equations describing the time evolution of JJAs and determine their fixed points for a few simple but instructive situations. We carry out generalizations of these results to larger arrays in Sec. III. In the final section, we summarize and discuss our findings.

II. PRELIMNARIES

The equation describing the dynamics of a single Josephson junction linking superconducting sites r and s, is given by the resistively and capacitively shunted junction (RCSJ) model [18,19] as

$$\beta_c \frac{d^2\phi_{rs}}{dt^2} + \frac{d\phi_{rs}}{dt} + \sin\phi_{rs} = i_{rs}, \tag{1}$$

where $\phi_{rs}=\phi_r-\phi_s$. The McCumber parameter β_c is defined as $2ei_cCR^2/\Phi_0$, where R is the shunt resistance, C is the shunt capacitance, i_c is the single junction critical current, and $\Phi_0=\hbar/2e$ is the flux quantum. The currents are scaled in terms of i_c and time is measured in units of $\hbar/2eRi_c$. We also recognize this equation as being that of a driven damped pendulum.

For an arbitary array, Eq. (1) applies separately to each junction, i_{rs} being the (instantaneous) dimensionless current it carries and ϕ_{rs} being the phase difference it supports. Conservation of total current implies that the i_{rs}'s must have zero divergence at each node of the array. Thus, for an $N_x\times N_y$ array of superconducting sites, connected by Josephson junctions, driven by external currents I^{ext}, the corresponding equations can be written using total current conservation (TCC) [20] as

$$\sum_{\langle rs\rangle}\beta_c\frac{d^2\phi}{dt^2}+\frac{d\phi_{rs}}{dt}+\sin\phi_{rs}=I_r^{ext}\quad\forall r, \tag{2}$$

where $\langle rs\rangle$ denotes summation over nearest neighbors of r. Note that ϕ_{rs} and hence Eq. (2), are invariant under $\phi_r\rightarrow\phi_r+\alpha$, where α is a constant. In solving Eq.(2) numerically, it is important to eliminate this freedom. This is easily done by setting the phase at an arbitrarily chosen site to zero.

Furthermore, $\Sigma\,\phi_{rs}=0$ identically, for a summation carried out around any closed path, or, in particular around a plaquette. If we restrict all phase differences to lie in the range $(-\pi,\pi]$ say, this condition must, however, be generalized to read $\Sigma\theta_{rs}=2\pi n(n=-1,0,1)$. This is used to identify the existence of a vortex in a plaquette.

In the fixed-point regime, $\ddot{\phi}_{rs}=\dot{\phi}_{rs}=0\;\forall r,s$ and, hence, $i_{rs}=\sin\phi_{rs}$. Our problem then is (1) To determine under what circumstances it is possible to find currents and phases consistent with the above constraints on the ϕ_{rs} and the i_{rs}, such that $i_{rs}=\sin\phi_{rs}$, for all junctions. (2) To examine the stability of the time-independent solutions so obtained.

For a single junction, we note that $\phi_{rs}=\sin^{-1}i_{rs}$ and $\phi_{rs}=\pi-\sin^{-1}i_{rs}$ are consistent time-independent solutions provided $i_{rs}\leqslant 1$. Of these the first is stable, whereas the second is not. For $i_{rs}>1$, a value of ϕ_{rs}, independent of time is not possible, i.e., $i_{rs}=1$ is the critical current for the single junction. We can reword these statements as follows. There is a one-to-one correspondence between the static configurations of a single junction and the values of $\phi_{rs}\equiv\phi\in[0,2\pi]$. We note that if ϕ is a solution corresponding to a given value of i_{rs}, then $-\phi$ is a solution for a current equal to $-i_{rs}$. We can, therefore, concentrate on $\phi\in[0,\pi]$. The current carried by the ϕ configuration is $\sin\phi$. When plotted against ϕ, this passes through a maximum of 1 at $\phi=\pi/2$. The configurations corresponding to a positive slope are stable whereas those for $di_{rs}/d\phi<0$ are unstable. A number of these observations generalize to larger arrays.

We next solve this problem in explicit detail for the triangular and square plaquette. Several features of these solutions will likewise be visible in arbitrarily large arrays.

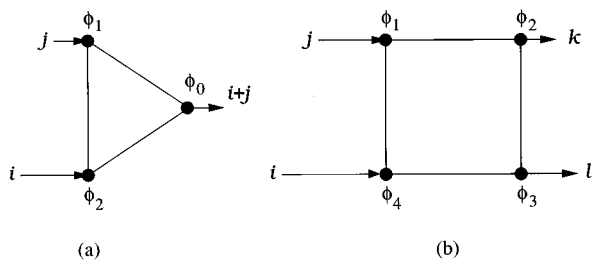

FIG. 1. Figure showing (a) a triangular and (b) a square plaquette. For the triangular plaquette, $\phi_0=0$ (by choice). Hence, $\phi_{10}=\phi_1$ and $\phi_{20}=\phi_2$. For the square plaquette, $\phi_{12}=\theta_1,\phi_{23}=\theta_2,\phi_{34}=\theta_3$ and $\phi_{41}=\theta_4$.

A. The triangular plaquette

For the triangular plaquette shown in Fig. 1(a), we choose $\phi_0=0$. Hence $\phi_{10}=\phi_1$ and $\phi_{20}=\phi_2$. The two independent phase differences for this configuration, thus, evolve according to the equations

$$3\frac{d\phi_1}{dt}=i+2j-2\sin\phi_1-\sin\phi_2-\sin(\phi_1-\phi_2)=f_1(\phi_1,\phi_2), \tag{3a}$$

$$3\frac{d\phi_2}{dt}=2i+j-\sin\phi_1-2\sin\phi_2+\sin(\phi_1-\phi_2)=f_2(\phi_1,\phi_2). \tag{3b}$$

These equations can be used to carry out a conventional linear stability analysis for the fixed point $(\overline{\phi_1},\overline{\phi_2})$ satisfying $f_r(\overline{\phi_1},\overline{\phi_2})=0,(r=1,2)$. We set $\phi_r=\overline{\phi_r}+\epsilon_r$, and arrive at the equation $\dot{\epsilon}_r=\Sigma_s\mathcal{M}_{rs}\epsilon_s$, where $\mathcal{M}_{rs}=(\partial f_r/\partial\phi_s)|_{\overline{\phi_1},\overline{\phi_2}}$.

The eigenvalue equation for the matrix, $\mathcal{M}_{rs}$, has the form

$$\lambda^2+b(\overline{\phi_1},\overline{\phi_2})\lambda+c(\overline{\phi_1},\overline{\phi_2})=0, \tag{4}$$

for specific functions b and c of (ϕ_1,ϕ_2). The fixed point becomes unstable when one of the λ's turns positive. The critical situation clearly corresponds to $b>0,c=0$. For Eqs. (3), these conditions read

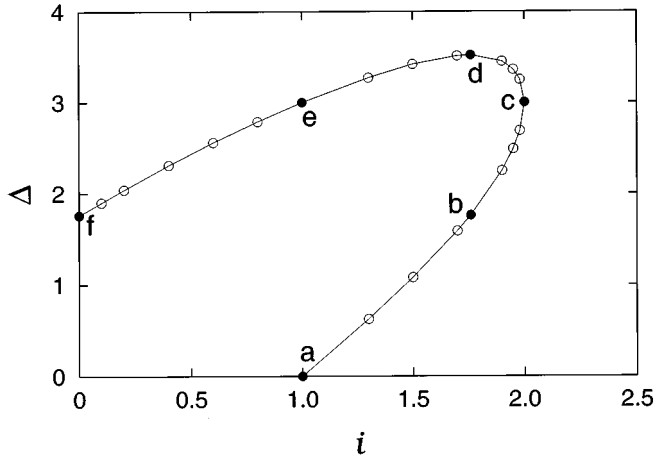

FIG. 2. Steady-state curve for the triangular plaquette in the (i,Δ) parameter space. Points a,b,c,d,e and f are intersections of the steady-state curve with lines on which the dynamics of the system is constrained by symmetry.

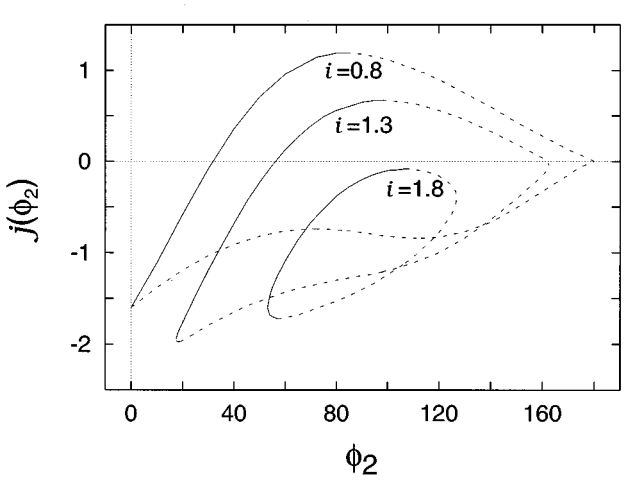

FIG. 3. A plot showing the variation of $j(\phi_2)$ as a function of ϕ_2 for the triangular plaquette. The solid line portions of the closed curves, shown for various values of i, correspond to stable fixed points of the system whereas the dashed line sections correspond to unstable ones.

$$\cos\phi_1+\cos\phi_2+\cos(\phi_1-\phi_2)>0, \tag{5a}$$

$$\cos\phi_1\cos\phi_2+\cos\phi_1\cos(\phi_1-\phi_2)+\cos\phi_2\cos(\phi_1-\phi_2)=0. \tag{5b}$$

We denote all (ϕ_1,ϕ_2) values satisfying these equations by (ϕ_{1c},ϕ_{2c}). Such points clearly lie on the critical curve. Translation from the (ϕ_1,ϕ_2) to the (i,j) variables can be carried out by means of the equations

$$j=\sin(\phi_1-\phi_2)+\sin\phi_1, \tag{6a}$$

$$i=\sin\phi_2-\sin(\phi_1-\phi_2). \tag{6b}$$

The critical curve Eq. (B5b) must, of course be plotted numerically and is shown in Fig. 2. A few points on it can, however, be identified by inspection. These are

(a) $\phi_{1c}=\phi_{2c}=\pi/2 (i=j=1)$,
(b) $\phi_{1c}=\phi_{2c}/2=53.13°\ldots(i=1.760\,172\ldots,j=0)$,
(c) $\phi_{1c}=0,\phi_{2c}=\pi/2 (i=2.0,j=-i/2)$,
(d) $\phi_{1c}=-\phi_{2c}/2=53.13°\ldots(i=1.760\,172\ldots,j=-i)$,
(e) $\phi_{1c}=-\pi/2,\phi_{2c}=0\ (i=1.0,j=-2i)$,
(f) $\phi_{1c}=2\phi_{2c}=-106.26°\ldots(i=0,j=1.760\,172\ldots)$.

Equations (5) and (6) can be understood from a different viewpoint. Let us fix i, such that $1\leqslant i\leqslant 2$. Then, for every value of ϕ_2, we get, from Eq. (6b), two values of ϕ_{12}—one in the first quadrant and one in the second. These, in turn, determine two values each for ϕ_1 and j [see Eq. (6a)]. By current conservation, the permitted range of ϕ_2 extends from $\sin^{-1}(i-1)$ to $\pi-\sin^{-1}(i-1)$ for $i>1$, while for $i\leqslant 1$, it becomes $[0,\pi]$. It is also useful to observe that ϕ_{12} passes from the first quadrant into the second at $\phi_{2\,min}$ and from the third to the fourth at $\phi_{2\,max}$. If we now plot j as a function of ϕ_2, we get a closed curve (see Fig. 3), which passes through a maximum of j_{max} and a minimum of j_{min}. Finally, varying Eqs. (6) with i fixed, shows that an increment δj of j is accommodated by changes $\delta\phi_r$ (in ϕ_r) which satisfy

$$\begin{pmatrix} \cos\phi_1+\cos(\phi_1-\phi_2) & -\cos(\phi_1-\phi_2) \\ -\cos(\phi_1-\phi_2) & \cos\phi_2+\cos(\phi_1-\phi_2) \end{pmatrix}\begin{pmatrix} \delta\phi_1 \\ \delta\phi_2 \end{pmatrix} = \begin{pmatrix} \delta j \\ 0 \end{pmatrix}. \tag{7}$$

A solution to Eqs. (7) exists, if and only if (iff) the matrix on the left-hand side (lhs) is nonsingular. If it is not, an increase in δj will necessarily make the flow resistive. Clearly the determinant, D_2, of this matrix is just the lhs of Eq. (B5b). It can also be easily checked from Eqs. (6) that the slope $dj/d\phi_2=D_2/\cos(\phi_1-\phi_2)$. Thus, D_2 is zero for $j=j_{max},j_{min}$ and is positive along the portion of the $j(\phi_2)$−curve, drawn with a solid line. The corresponding values of (ϕ_1,ϕ_2) represent stable configurations while those along the dashed portion represent unstable ones. An inspection of Fig. 3 further shows that at j_{max}, stable and the unstable fixed points merge and for still larger or smaller values of j, respectively, there is no stationary solution.

In slightly more intuitive terms, the existence of j_{max} and j_{min} can be explained as follows. If we increase j, keeping i fixed, $(1<i<2)$, ϕ_1 and ϕ_2 both increase $(\phi_2>\phi_1)$. As a result ϕ_2 eventually enters the second quadrant, i.e., we have $\phi_1<\pi/2<\phi_2$. Once this happens $\sin\phi_2$ starts decreasing with increasing j while $\sin\phi_1$ continues to increase, of course. In time, we reach a point at which the decrease in $\sin\phi_2$ exactly matches the increase in $\sin\phi_1$ and j can be raised no further. Similarly, j_{min} comes about when j turns negative, i.e., we are extracting current, and ϕ_{12} begins increasing inside the second quadrant while ϕ_2 increases in the first.

B. The square plaquette

We now take up the case of a single square plaquette, driven by direct currents i,j,k and $l(i+j=k+l)$ as shown in Fig. 1(b). The configurational variables for this network are $\phi_{12}=\theta_1,\phi_{23}=\theta_2,\phi_{34}=\theta_3$, and $\phi_{41}=\theta_4$, of which only

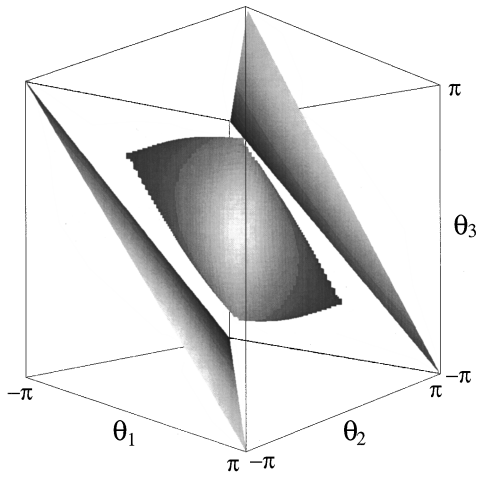

FIG. 4. Figure showing the critical surface in the $(\theta_1,\theta_2,\theta_3)$ space for a square plaquette. The surface lies in between the two planes representing the boundaries of the positive and negative vortex regions.

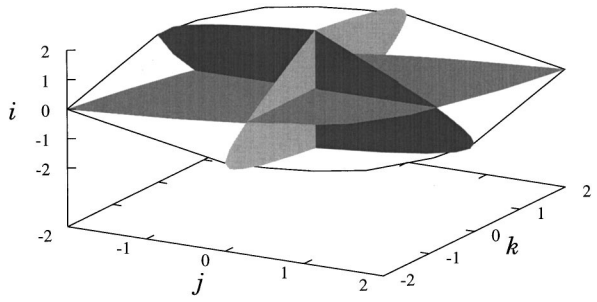

FIG. 5. The critical surface enclosing the fixed-point region, for the square plaquette, in the (i,j,k) parameter space. The $i=0$, $j=0$ and $k=0$ projections are prominently shown by the shaded planes.

three, say $\theta_i (i=1,2,3)$, are independent for any given vortex sector. It can easily be shown, through the techniques employed for the triangular plaquette, that the critical boundary, in this case, is given by

$$\cos\theta_1\cos\theta_2\cos\theta_3+\cos\theta_2\cos\theta_3\cos\theta_4+\cos\theta_3\cos\theta_4\cos\theta_1 + \cos\theta_4\cos\theta_1\cos\theta_2=0 \tag{8}$$

and the lhs>0, for all points enclosed by the surface so defined. This surface is shown in Fig. 4, and is seen to be well away from from the vortex regions, which now correspond to $\theta_1+\theta_2+\theta_3>\pi$ for positive vortices and $\theta_1+\theta_2+\theta_3<-\pi$ for negative ones.

Moreover, since a choice of $(\theta_1,\theta_2,\theta_3)$ automatically fixes the external currents i,j,k, Eq. (8) defines a critical surface in (i,j,k) space as well. The $i=0$, $j=0$, and $k=0$ sections of this surface are displayed in Fig. 5. In mapping out this surface, it is helpful to note that there are, as for the triangular plaquette, a number of special rays in (i,j,k) space for which the critical point is easily determined, e.g.,

(a) $\theta_1=\theta_3;\theta_2=\theta_4=0\ (i=j=k)$,
(b) $\theta_2=-\theta_3=-\theta_4 (i=k=0;j=l)$,
(c) $\theta_1=\theta_4;\theta_2=\theta_3 (j=0,k=0;i=l)$,
(d) $\theta_1=-\theta_2;\theta_3=-\theta_4 (j=k=l=i/3)$,
(e) $\theta_1=\theta_2=0;\theta_3=-\theta_4 (j=k=i/2,l=0)$.

It is also worth emphasizing that the critical surface in current space captures *all* values of external drive for which a transition from superconductive to resistive flow takes place for the given network. What is more, if we extend the single plaquette into a horizontal *ladder*, the critical surface remains unaltered provided we take k to be the current, flowing out of the upper corner of the leftmost plaquette. This current k will, of course, now be a function of the external currents, which should for clarity be relabeled at this stage as i_{ext}, j_{ext} and k_{ext}. If we choose to short the current extraction edge with a bus-bar, k_{ext} ceases to be independently adjustable and $k(i_{ext}\equiv i, j_{ext}\equiv j)$ defines a two-dimensional surface in (i,j,k) space, whose intersection with the critical surface produces the curve along which the ladder goes critical. This curve depends, in principle, on the length of the ladder, but changes, in practice, very little beyond $n=4$.

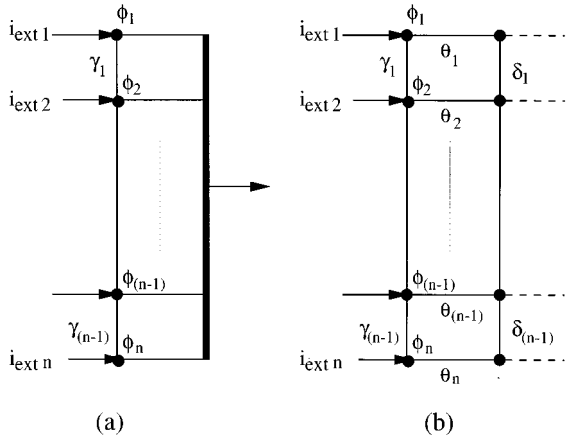

FIG. 6. (a) The column of a $2\times n$ array shorted on the right and (b) the leftmost column of a rectangular array (the currents drawn out are not shown).

III. GENERALIZATIONS TO LARGER ARRAYS

Our next task is to generalize these arguments to larger arrays. It is expedient to do this by first considering vertical ladders and only then moving onto rectangular arrays, with and without missing bonds.

The fixed-point behavior of a $(2\times n)$ array, shorted on the right, i.e., a column of triangles (see Fig. 6), is governed by the equations

$$i_{ext\,1}=\sin\phi_1+\sin\gamma_1, \tag{9a}$$

$$i_{ext\,2}=\sin\phi_2+\sin\gamma_2-\sin\gamma_1, \tag{9b}$$

$$\vdots$$

$$i_{extn}=\sin\phi_n-\sin\gamma_{n-1}, \tag{9c}$$

where $\gamma_r=\phi_r-\phi_{r+1},\forall r$. The phase, ϕ_0, along the bus-bar is held fixed at zero and treated as a point of reference.

To find the critical hypersurface for this ladder, we vary Eqs. (9) to get a matrix equation of the form $\Sigma_{s=1}^{n} M_{rs}^{(n)}\delta\phi_s=\delta i_{extr}$, and set $D_n=\det M^{(n)}=0$. It can be checked that D_n is proportional to the *determinant* of the matrix $\mathcal{M}^{(n)}$ which governs the time evolution of small perturbations, ϵ_r $(r=1,2,\ldots,n)$, about the fixed point, $\{\phi_r\}$: $\dot{\epsilon}_r=\Sigma_{s=1}^{n}\mathcal{M}_{rs}^{(n)}\epsilon_s$. Moreover, the proportionality constant contains a factor of $(-1)^n$. Now the stability of $\{\phi_r\}$ requires that all n eigenvalues of $\mathcal{M}^{(n)}$ be negative. Hence, a necessary (but not sufficient) condition for the stability of the fixed point is $D_n(\{\phi_i\})>0$. The sufficiency conditions involve determinants of submatrices of $M^{(n)}$. For example, for the (2×2) case discussed above, conditions (5a) and (5b), i.e., $D_2>0$ along with the tracelessness of $\mathcal{M}^{(2)}$, *taken together* ensure sufficiency. This is because eigenvalues changing signs in pairs keep D_n positive. For our purposes, it suffices to delineate a surface on which $D_n=0$ and *inside* which D_n is everywhere positive.

The form of $M^{(n)}$ can readily be determined inductively. Indeed, we can clearly pass from the $M^{(n-1)}$ to $M^{(n)}$ by adding $\cos\gamma_{n-1}$ to the $(n-1)^{th}$ diagonal element of $M^{(n-1)}$

and appending to the matrix so obtained, an extra row and column, with all elements set to zero other than

$$M^{(n)}_{n-1,n}=M^{(n)}_{n,n-1}=-\cos\gamma_{n-1},$$

$$M^{(n)}_{n,n}=\cos\gamma_{n-1}+\cos\phi_n.$$

We note that $M^{(n)}$ is a tridiagonal matrix.

D_n can be easily checked to likewise have the inductive form

$$A_1=1, \quad D_1=\cos\phi_1, \tag{10a}$$

$$A_n=D_{n-1}+A_{n-1}\cos\gamma_{n-1}, \tag{10b}$$

$$D_n=(\cos\phi_n+\cos\gamma_{n-1})D_{n-1}+A_{n-1}\cos\phi_n\cos\gamma_{n-1}. \tag{10c}$$

These equations accord a recursive evaluation of D_n in linear order. We note that $n=1$ corresponds to a single junction and that for, $n=2$, Eq. (10c) reduces to the lhs of Eq. (5b). Furthermore, when written out explicitly D_n is the sum of all products of n cosines of phase differences, chosen such that the corresponding bonds do *not* form closed curves. For $i_{extr}=0\forall r$, i.e., at what is, in some sense, the most stable point in parameter space, D_n has its maximum value of n, whereas on the critical surface $D_n=0$. We can thus view D_n as an order parameter for the superconductive to resistive transition and usefully incorporate it into a program for the numerical integration of Eqs. (2), as a sensitive measure of the distance from criticality, *inside* the fixed-point regime. Its utility persists even in the time-dependent domain (where it is initially negative), since it varies more rapidly in the neighborhood of the critical hypersurface than the magnitude of $d\phi/dt$, which is another obvious measure of deviation from criticality.

We reemphasize that the critical hypersurface we have defined bounds the entire set of fixed points of Eqs. (9), provided the drive keeps the equations autonomous. The n dimensionality of this surface is the unavoidable price of keeping the external drive completely general: Any restriction on the latter, quite generally tends to lower the dimensionality of the former and is effectively equivalent to viewing the surface along specific sections. To make analytic use of or, in fact, to just meaningfully interpret Eqs. (10), the importance of such and other sections cannot be overemphasized.

For example, by considering the critical $\phi_n=\pi/2$ sections, we can straightforwardly deduce from Eqs. (10) that a configuration stable for a $2\times(n-1)$ ladder, can always be stably embedded into a $2\times n$ ladder. Indeed, assume, for simplicity, that the configuration is critical, i.e., $D_{n-1}=0$. If we choose $\phi_n=\pi/2$ or $\phi_n=\phi_{n-1}-\pi/2$, then $D_n=0$ trivially. In other words, the $\phi_n=\pi/2$ and $\gamma_{n-1}=\pi/2$ sections of the $2\times n$ critical surface coincide with the $2\times(n-1)$ critical surface. The external current must be appropriately adjusted, of course, but since these are not constrained in any way, this is always possible. This further implies that the range of (ϕ_1,ϕ_2) values (i.e., those defining configurations of the first plaquette), lying inside the fixed-point regime of a $2\times n$ ladder is at least as large as that for a $2\times(n-1)$ ladder. We have numerically checked that this range, in fact, increases slowly.

It is also worth mentioning that in some cases induction allows us to extract nontrivial information from Eqs. (10). We can show, for instance, that if the ladder is subjected to a monotonically decreasing current profile (i.e., to $i_1>i_2>\cdots>i_n$, which ensures that $\phi_1>\phi_2>\cdots>\phi_n$), time dependence sets in long before ϕ_1 reaches the value of π, i.e., before a vortex can form in the top plaquette of the array. Indeed, if $\phi_1>\phi_2>\cdots>\phi_n$, then at criticality only the first few ϕ's can be in the second quadrant. (This can be deduced by arguments analogous to those given in Sec. II for the triangular plaquette.) Furthermore, with $\phi_1=\pi$, $D_2=-\cos^2\phi_2$ and $A_2=\cos\gamma_1-1<0$. Consequently, ϕ_n and γ_{n-1} will be in the first quadrant. If we now assume that D_{n-1} and A_{n-1} are both nonpositive, then Eqs.(10b) and (10c) straightaway imply that $D_n, A_n\leqslant 0$ (but are not *both* zero simultaneously). We have already seen that $D_n>0$ is a *necessary* condition for stability. Thus for all ladders, regardless of length, the statement we set out to prove, holds.

It is interesting that the critical hypersurface for an *arbitrary* dc-driven rectangular array can be determined by only a slight extension of the arguments pertaining to the vertical ladder. It is sufficient to observe that the column at the drive edge bears the full brunt of the external current input. If it remains nonresistive, then the rest of the array finds itself driven by direct currents, each of value less than unity (since these must be the *sines* of some angle or other). Such drives can, of course, be handled without introducing any time dependence. Thus the stability of the entire array depends on that of the leftmost column (see Fig. 6). The determinant describing the critical hypersurface of this column can, as above, be readily put down by induction

$$A_1=1, \quad D_1=\cos\theta_1, \tag{11a}$$

$$A_n=(\cos\gamma_{n-1}+\cos\delta_{n-1})D_{n-1}+A_{n-1}\cos\gamma_{n-1}\cos\delta_{n-1}, \tag{11b}$$

$$D_n=(\cos\theta_n\cos\gamma_{n-1}+\cos\gamma_{n-1}\cos\delta_{n-1}+\cos\delta_{n-1}\cos\theta_n)]\times D_{n-1}+A_{n-1}\cos\theta_n\cos\gamma_{n-1}\cos\delta_{n-1} \tag{11c}$$

where $\theta_m=\phi^1_{(m)}-\phi^2_{(m)}$, $\gamma_{m-1}=\phi^1_{(m-1)}-\phi^1_{(m)}$, $\delta_{m-1}=\phi^2_{(m-1)}-\phi^2_{(m)}$, and $\phi^r_{(m)}$ are the phases along the mth row of the array. We note that the central defect corridor of an array with a linear defect (the central column of an array with a number of broken row bonds) represents a special case of Eqs. (10). In this case, the phases along the right edge of this corridor are the negatives of those along the left edge, whence $\gamma_{m-1}=-\delta_{m-1}$.

Analytic information can be extracted from Eqs. (11) by using projections and induction in much the same way as above. Rather than discussing further illustrations of such projections taken in terms of *phases*, we end this section with a projection taken in terms of the external *currents*. Since these currents are what we manipulate in experiments, such projections are clearly the ones which are more directly physical. The case we consider is that of a drive, varying linearly between a maximum of i and a minimum of j $(i>j)$. This clearly corresponds to a two-dimensional pro-

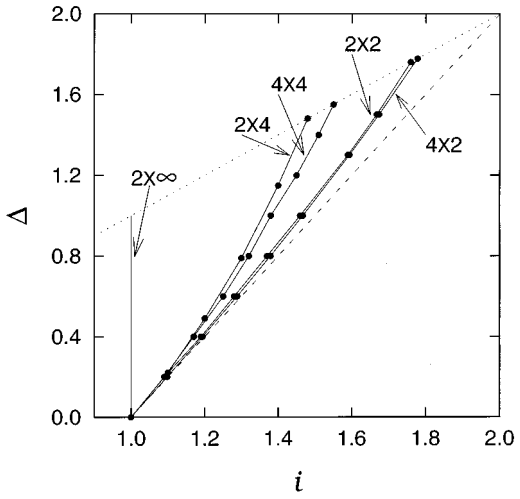

FIG. 7. Typical transition curves, in the (i,Δ) space bounding the steady-state regions for various array sizes marked against the curves. The dotted and the dashed lines represent the $j=0$ and $i+j=2$ lines, respectively. All curves lie between $C_{2\times\infty}$ and $C_{\infty\times 2}$.

jection of the n-dimensional critical surface defined in Eqs. (10) and Eqs. (11). It leads to a family of critical curves, some members of which have been displayed in Fig. 7. These curves reflect the following properties of ladders and rectangular arrays:

(1) If currents (i,j) can flow nonresistively through an array then $(i'<i,j'<j)$ can flow nonresistively as well. Since $i=j=1$ can always be passed through the array, the region to the left of line $i=1$ (Fig. 7) always lies in the steady state for all arrays. (2) The largest time-independent flow of current through an array occurs for $i=j=1$. Thus all critical curves lie to the left of the $i+j=2$ line and meet it at $i=1$. (3) If (i,j) is a fixed point of a row of m plaquettes then it is also a fixed point of a row of n plaquettes, $n>m$. The critical curve, $C_{n\times 2}$ of an $n\times 2$ array therefore lies to the right of $C_{m\times 2}$. We shall denote this by writing $C_{n\times 2}>C_{m\times 2}$.

To get some feeling for this property, we note that for a $(n\times 2)$ array (n arbitrary), the gradient in the y direction reduces as we move rightwards, i.e., away from the drive edge . However, the gradient never becomes exactly zero, for if it did at some plaquette l, the phase differences around the latter would read $(\gamma_l,\phi_l,0=\gamma_{l+1},-\phi_l=\beta_l)$ and would not sum to zero.

If we now add an extra plaquette on the right, γ_{n+1}, which was earlier zero (being the phase difference across the shorted junction) assumes a positive value and forces all the phases to readjust themselves. We could, equivalently give γ_{n+1} its nonzero value by injecting at the site $(n,0)$ a current $-i'$, satisfying $\sin^{-1}(i_n-i')-\sin^{-1}(j_n+i')=\gamma_{n+1}$, and withdrawing it from site $(n,1)$. In going from source to sink, $-i'$, could reasonably be expected to cycle through all the vertical bonds, in amounts which decrease monotonically as we move away from the point of injection. This would push up all the $\gamma_i(i=(n+1),\ldots,2)$ such that $\triangle\gamma_{i+1}>\triangle\gamma_i$ and, furthermore, would raise the β_i and depress the ϕ_i, to achieve consistency with $\triangle(\phi_i-\beta_i)=\triangle(\gamma_i-\gamma_{i+1})$.

Thus as far as the plaquette next to the drive edge is concerned, adding a plaquette tends to enhance γ_2, while removing one depresses it. For fixed (i,j), $\gamma_2=\sin^{-1}[i+j-\sin\phi_1]+\sin^{-1}[i-\sin\phi_1]-\phi_1$. If we plot $\gamma_2(\phi_1)$ versus ϕ_1, we find that it goes through a minimum. Thus a larger value of γ_2 is always possible while a smaller value may or may not be. Hence, the above results.

It follows that $C_{\infty\times 2}=\lim_{n\to\infty}C_{n\times 2}>C_{m\times 2}\forall m$. Convergence to the limiting curve is very rapid, e.g., for $j=0$, the point of maximal separation between curves, $i_{max}=$ 1.7601, 1.7782, 1.7787, and 1.778 78 for $n=2,3,4$, and 6, respectively. For all arrays with $n>6$, changes in i_{max} are confined to the fifth place of decimal or beyond. For most purposes $n=4$ is large enough.

(4) $C_{2\times n}<C_{2\times m}$ if $n>m$ and $\lim_{n\to\infty}C_{2\times n}$is the line $i=1$. To prove the latter, let us suppose that $\lim_{n\to\infty}i_{max}(2\times n;j=0)=1+\epsilon$, $\epsilon>0$. Then for an arbitary number $m>0$, any column of length $n>m(1+1/\epsilon)$ would have m input currents exceeding unity. The $(m+1)$th vertical bond will then carry a current equal to $\Sigma_{p=1}^{m}(i_{extp}-\sin\phi_p)$, where $\phi_p=\phi_1-\Sigma_{i=1}^{p-1}\gamma_i$ for $\gamma_i>0,\forall i$. This current can be made to exceed unity for m sufficiently large. This argument also indicates that ϵ must decrease continuously as we increase the size of the column. (5) $C_{2\times m}<C_{n\times m}<C_{n\times 2}$ for $n,m>2$.

IV. SUMMARY AND DISCUSSION

To summarize, we have carried out, from first principles, the fixed-point analysis of dc-driven Josephson junction arrays at zero temperature and zero magnetic field. We have discussed isolated triangular and square plaquettes in exhaustive detail and understood their fixed-point behaviors from several viewpoints. We have, moreover, put down closed-form inductive expressions for the critical surfaces of ladders of arbitrary length, as also of rectangular arrays of arbitrary size. The latter was made possible by the fact that the time-independent behavior of a two-dimensional JJA is determined by that of a single column, namely, the one at the drive edge for a perfect array, and the defect corridor for arrays with linear defects. A reduction of the problem to anything smaller than this column is not possible because the external currents can be adjusted independently and junctions driven by them are, moreover, globally coupled. Finally, we have provided illustrations of how various projections of the critical surface can be made to yield useful information about the system. We have considered projections in terms of both phases and currents. In discussing the latter, we plotted, for a drive with a linearly varying profile, the curves in (i,Δ) space, along which a transition to time dependent, resistive current flow occurs.

We emphasize that our analysis has been carried out entirely in terms of *phase* as opposed to *vortex* variables (in terms of which, JJAs enjoy an alternative description). To the extent that vortices can be checked numerically to be unstable inside ladders with bus-bars (i.e., the repulsion by the latter exceeds the pinning potential of the lattice) and inside isolated square plaquettes, our treatment of these configurations is essentially complete. For the multivortex sectors of large arrays, with and without missing bonds, however, the effective description may actually be quite useful. Developing this approach to the point where it yields precise

quantitative information about the stability of vortices is an important direction for future research.

It is further worth mentioning that the inclusion of inductances and capacitances for the junctions of the array does not, for obvious reasons, alter the fixed points of the system. However, as pointed out in the introduction, switching on a magnetic field *would*. The ground states in the presence of such fields, of an external current-free system *have* been studied extensively. The results of this paper can now be combined with those studies, to analyze what happens in the presence of *both* external current drives and magnetic fields.

As for a finite temperature, this will introduce thermally generated vortex antivortex pairs. As soon as these are set into motion by an external current drive, they will cause a breakdown of superconductive flow. A quantitative study of these fluctuations, through the introduction of noise or by Monte Carlo techniques, is yet another investigation which can now be meaningfully undertaken.

To conclude, the straightforward analysis carried out in this paper has not only accorded us several qualitative insights into the time-independent behavior of JJAs, but has also shown that despite the large number of variables characterizing these systems, their quantitative fixed-point behavior is quite tractable.

[1] Proceedings of the NATO Advanced Research Workshop on Coherence in Superconducting Networks, Delft, The Netherlands, December 1987, edited by J. E. Mooij and G. B. J. Schon [Physica B **152**, 1 (1988)].
[2] M. Tinkham, D. W. Abraham, and C. J. Lobb, Phys. Rev. B **28**, 6578 (1983).
[3] Ch. Leemann, Ph. Lerch, and P. Martinoli, Physica B **126**, 475 (1984).
[4] R. Voss and R. Webb, Phys. Rev. B **25**, 3446 (1982).
[5] J. Carini, Phys. Rev. B **38**, 63 (1988).
[6] M. G. Forrestor, H. J. Lee, M. Tinkham, and C. J. Lobb, Phys. Rev. B **37**, 5966 (1988).
[7] H. S. J. van der Zant, F. C. Fritschy, T. P. Orlando, and J. E.Mooij, Europhys. Lett. **18**, 343 (1992).
[8] P. L. Leath and W. Xia, Phys. Rev. B **44**, 9619 (1991).
[9] K. K. Mon and S. Teitel, Phys. Rev. Lett. **62**, 673 (1989).
[10] F. Falo, A. R. Bishop, and P. S. Lomdahl, Phys. Rev. B **41**, 10 983 (1990).
[11] R. Mehrotra and S. R. Shenoy, Phys. Rev. B **46**, 1088 (1992).
[12] Shantilal Das, Sujay Datta, Mitrajit Dutta, Shilpa Jain, and Deshdeep Sahdev, Physica D **91**, 278 (1996); Shantilal Das, Sujay Datta, M. K. Verma, Deshdeep Sahdev, and Ravi Mehrotra, *ibid.* **91**, 292 (1996) .
[13] Shantilal Das, Sujay Datta and Deshdeep Sahdev, Physica D (to be published).
[14] Sujay Datta, Shantilal Das, Deshdeep Sahdev, and Ravi Mehrotra, Mod. Phys. Lett. **10**, 451 (1996).
[15] D. Dominguez and J. V. José, Phys. Rev. Lett. **69**, 514 (1992).
[16] C. J. Lobb, David W. Abraham, and M. Tinkham, Phys. Rev. B **27**, 150 (1983).
[17] For complete accuracy, we should mention that uniformly driven perfect arrays do not follow the pattern above, but then they behave in all respects like a parallel set of linear arrays, decoupled from one another and are, in this sense, not quite two dimensional.
[18] W. C. Stewart, Appl. Phys. Lett. **12**, 277 (1968).
[19] D. E. McCumber, J. Appl. Phys. **39**, 3113 (1968).
[20] S. R. Shenoy, J. Phys. C **18**, 5163 (1985); **20**, 2479(E) (1987).